Smectic-C^*_α phase with two coexistent helical pitch values and a first-order smectic-C^*_α to smectic-C^* transition

B. K. McCoy,[1] Z. Q. Liu,[1] S. T. Wang,[1,2] R. Pindak,[2] K. Takekoshi,[3] K. Ema,[3] A. Seed,[4] and C. C. Huang[1]
[1]*School of Physics and Astronomy, University of Minnesota, Minneapolis, Minnesota 55455, USA*
[2]*NSLS,Brookhaven National Laboratory, Upton, New York 11973, USA*
[3]*Department of Physics, Graduate School of Science and Engineering, Tokyo Institute of Technology, 2-12-1 O-okayama, Meguro, Tokyo 152-8550, Japan*
[4]*Chemistry Department, Kent State University, Kent, Ohio 44242, USA*
(Received 1 March 2007; published 24 May 2007)

Previous results from Kundu *et al.* using dielectric relaxation have suggested a reentrant antiferroelectric-ferroelectric-antiferroelectric transition in the compound LN36. Our comprehensive studies of this compound using differential optical reflectivity, nonadiabatic scanning calorimetry, null transmission ellipsometry, and resonant x-ray diffraction show that in fact LN36 exhibits the usual phase sequence for chiral smectic liquid crystals: SmA^*-SmC^*_α-SmC^*-SmC^*_{FI1}-SmC^*_A. Moreover, the SmC^*_α-SmC^* transition is a first-order transition, characterized by a discontinuous change in the helical pitch. At temperatures just above the SmC^*_α-SmC^* transition, two different values for the helical pitch are simultaneously observed for the first time.

DOI: 10.1103/PhysRevE.75.051706 PACS number(s): 64.70.Md, 77.84.Nh

I. INTRODUCTION

Determination of the detailed structure of the smectic-C^* (SmC^*) variant phases of chiral molecules has required immense efforts using several experimental tools. Still many questions remain regarding the transitions between the phases. The typical phases of interest in the liquid crystal regime are smectic-A^* (SmA^*) in which the molecular axes are on average parallel to the layer normal and various SmC^* variant phases in which the molecular long axes are tilted away from the layer normal. In the SmC^* variant phases the tilt directions in successive layers may form the smectic-C^*_α (SmC^*_α) phase with an incommensurate helical pattern with pitch on the order of ten smectic layers, ferroelectric smectic-C^* (SmC^*) with a long helical pitch, smectic-C^*_{FI2} (SmC^*_{FI2}) and smectic-C^*_{FI1} (SmC^*_{FI1}), with commensurate progressions of the tilt axis with four or three layer unit cells in the distorted clock model [1], or antiferroelectric smectic-C^*_A (SmC^*_A), with the tilt directions antiparallel in adjacent layers. These phases typically occur in the same order for all compounds, though some phases may be missing for some compounds [2]. The SmA^*-SmC^*_α transition is second order. The transition from SmC^* to any of the commensurate phases, SmC^*_{FI2}, SmC^*_{FI1}, or SmC^*_A, is first order [3]. The transition from SmC^*_α to SmC^* is first order ending at a critical point [4].

Kundu *et al.* have performed temperature and frequency dependent dielectric relaxation measurements on the compound LN36, revealing antiferroelectric-ferroelectric-antiferroelectric behavior [5]. Though they presume that the antiferroelectric phases are SmC^*_A, the identity of the phases was not demonstrated conclusively. In this paper, we present data on LN36 using differential optical reflectivity (DOR), nonadiabatic scanning (NAS) calorimetry, null transmission ellipsometry (NTE), and resonant x-ray diffraction (RXRD). The chemical structure of LN36 is shown in Fig. 1. The phase sequence for LN36, determined by our four experimental probes is SmA^*(388.2 K)SmC^*_α(387.6 K) SmC^*(380.2 K)SmC^*_{FI1}(378.0 K)SmC^*_A-crystal. In addition, the SmC^*_α-SmC^* transition is shown to be a first-order transition, with two coexistent values of the pitch in the SmC^*_α phase just above the transition.

II. DIFFERENTIAL OPTICAL REFLECTIVITY

In DOR, 633 nm laser light linearly polarized by a Glan-Thompson polarizer is incident at a 13.9° angle on a free-standing liquid crystal film. A detailed description of our DOR apparatus can be found in Ref. [6]. The reflected light passes through a polarizing beam splitter, separating the $\hat{p}$ and $\hat{s}$ components. The intensities of the reflected $\hat{p}$ and $\hat{s}$ components are measured by two photodetectors. The two signals are added or subtracted electronically then amplified to give two measured parameters I_P+I_S and I_P-I_S. The total reflectivity I_P+I_S is related to the thickness of the film. Because of the oblique incidence, some differential reflectivity occurs between the $\hat{p}$ and $\hat{s}$ components. When the film is in the optically uniaxial SmA^* phase, the Glan-Thompson polarizer is rotated away from 45° from the incident plane until $I_P-I_S=0$ to compensate for the effect of the thickness on the differential reflectivity. When the film is subsequently cooled into the biaxial tilted smectic phases, the biaxiality causes additional differential reflectivity of the $\hat{p}$ and $\hat{s}$ components, giving rise to an I_P-I_S signal. The I_P-I_S signal is determined by the magnitude of the biaxiality and the orientation of the optical axis with respect to the incident plane.

The dependence of the I_P-I_S signal on the orientation of the optical axis makes DOR a particularly useful tool for studying the SmC^*_α phase. The helical pitch of the SmC^*_α

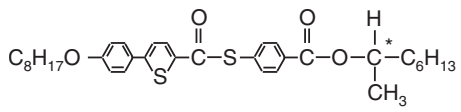

FIG. 1. Chemical structure of LN36.

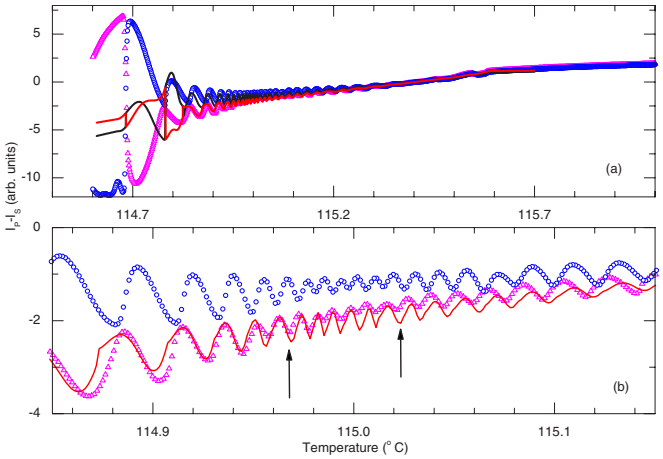

FIG. 2. (Color online) (a) $I_P - I_S$ vs T with the electric field parallel to (magenta triangles) and perpendicular to (blue circles) the projection of the incident wave vector on the layer plane. The solid lines are simulation results for the two directions of the electric field as described in the text. The simulation is only shown for one direction of the electric field in (b) for clarity. (b) shows the SmC^*_α-SmC^* transition region in a smaller temperature window. The arrows mark the region with increased frequency and decreased amplitude of oscillations as discussed in the text.

phase depends on temperature; as the temperature changes, the number of turns of the helix and the orientation of the molecules at the surfaces of the film change, giving rise to oscillations in the $I_P - I_S$ signal as a function of temperature. The freestanding films are anchored to the edges of a 7 mm hole in a glass coverslip. Electrodes on the glass apply an electric field of approximately 2.9 V/cm either parallel or antiparallel to the projection of the incident wave vector on the film plane. The applied electric field stabilizes a monodomain sample and aligns the net polarization of the film without distorting the internal structure of the phase. Figure 2 shows data for a 429±1 layer film while cooling at 10 mK/min with the electric field parallel and antiparallel to the projection of the incident wave vector on the film plane. Above 115.58 °C, the film is in the SmA^* phase. As the tilt increases below the SmA^*-SmC^*_α transition, $I_P + I_S$ changes as shown in Fig. 3 because the film thickness decreases. The thickness is such that a minimum in the reflectivity occurs at

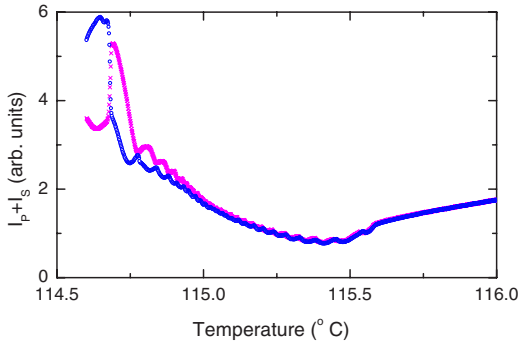

FIG. 3. (Color online) $I_P + I_S$ vs T with the electric field parallel to (magenta crosses) and perpendicular to (blue circles) the projection of the incident wave vector on the layer plane.

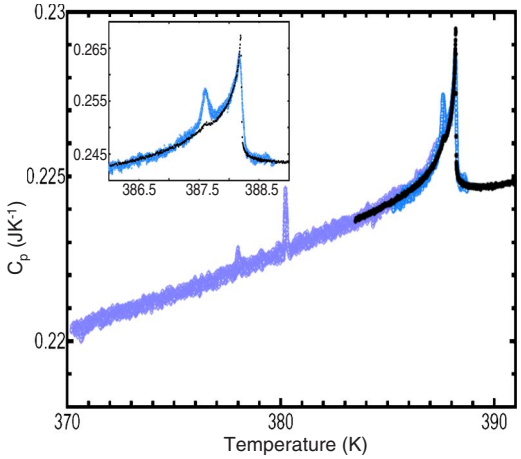

FIG. 4. (Color online) (a) Calorimetry data in the NAS mode (blue, entire temperature range) and AC mode (black, above 384.5 K). The inset shows the SmC^*_α-SmC^* transition region in more detail. A faster temperature scanning rate was used in the NAS mode below the temperature range shown in the inset. The anomaly at 387.6 K does not appear in the AC mode.

about 0.2 °C below the SmA^*-SmC^*_α transition. Oscillations in $I_P + I_S$ also occur as the biaxiality of the film changes. Each oscillation in $I_P + I_S$ and $I_P - I_S$ corresponds to a change by one in the number of turns of the SmC^*_α helix. From the large number of oscillations present, we can deduce that the pitch must be increasing as temperature decreases. The magnitude of the helical pitch will be determined later by other methods. The amplitude of the oscillations increases as the tilt angle increases. The region from 115.03 °C to 114.98 °C is of particular interest; the frequency of the oscillations increases dramatically, indicating that the pitch changes rapidly with temperature, and the amplitude of the oscillations decreases. Similar features were observed in several films. This surprising behavior in DOR served as motivation for our continued experiments on LN36.

III. CALORIMETRY

Heat capacity data are shown in Fig. 4. The sample was placed in a hermetically sealed gold cell with a weak thermal connection to a temperature controlled bath. The heat capacity was measured by linearly ramping the heating power applied to the sample cell in the NAS mode or varying the power sinusoidally in the alternating current (AC) mode, while observing the sample temperature [7,8]. The data include the heat capacity of the cell, which depends linearly on the temperature. The large peak at 388.2 K marks the SmA^*-SmC^*_α transition. The remaining anomalies occur at the transitions to SmC^* (387.6 K), SmC^*_{FI1} (380.2 K), and SmC^*_A (378.0 K). The identities of these phases will be established later using NTE and RXRD. Both NAS and AC modes were used to measure the heat capacity anomalies from the SmA^* phase to the SmC^* phase. In the inset to Fig. 4, the two modes are in good agreement across the SmA^*-SmC^*_α transition but only the NAS mode shows a significant signal at the SmC^*_α-SmC^* transition. A plausible ex-

planation for the lack of an anomaly in the AC mode signal at the SmC^*_α-SmC^* transition is that this is a first-order transition, as the AC mode is not sensitive to small latent heats. The SmC^*_α-SmC^* heat capacity anomaly is much larger than the anomaly observed in previous compounds that have shown first-order SmC^*_α-SmC^* transitions. The data shown in Fig. 4 was obtained while cooling; another run while heating showed a small hysteresis, 40 mK, in the peak of the SmC^*_α-SmC^* anomaly.

IV. NULL TRANSMISSION ELLIPSOMETRY

When polarized light is transmitted through a freestanding film, the elliptical polarization state changes. Our null transmission ellipsometer arranges for a null transmission state in the polarizer-compensator-sample-analyzer configuration [9,10]. Elliptically polarized 633 nm laser light, with the elliptical state set by the orientation of the polarizer with respect to the compensator's easy axis, is incident on a freestanding film at a 45° angle with the film normal. The ellipticity of the incident light is arranged so that the transmitted light is linearly polarized. The analyzer then measures the polarization direction of the transmitted light. Two parameters Ψ and Δ give the phase lag between the $\hat{p}$ and $\hat{s}$ components of the incident light necessary to give linearly polarized transmitted light and the direction of the analyzer axis, respectively. The film is in an oven with temperature stability of 10 mK. The freestanding film is prepared across a hole in a glass film plate that is similar to the DOR film plate. A rotatable electric field is applied by eight electrodes spaced symmetrically around the film hole.

By holding the temperature constant while changing the direction of the electric field, we can probe the symmetry of the phase with respect to rotations about the film normal. Figure 5 shows data for Ψ and Δ as a function of α, the angle between the electric field vector and the incident plane. At 117.5 °C [Fig. 5(a)], the spans of the Ψ and Δ curves are relatively small; the film is in the uniaxial SmA^* phase. The dependence of Ψ and Δ on α is due to the presence of tilted surface layers. Since only one minimum in Δ is present, at α=270°, the tilt is in the same direction in all surface layers. Both Ψ and Δ depend much more strongly on α at 112.9 °C [Fig. 5(b)]; the film is biaxial. Again Δ has only one minimum so the phase is SmC^*. Two asymmetric minima in Δ at 108.9 °C [Fig. 5(c)] indicate that the phase is no longer SmC^*. The identity of the phase cannot be determined definitively from the NTE data, though asymmetry in the Δ vs α curve suggests that it is SmC^*_{FI1} [11]. Cooling further to 99.7 °C [Fig. 5(d)], the angular locations of the minima in Δ shift by 90° due to a change in the direction of the net polarization and the Δ vs α curve becomes much more symmetric. This phase is likely SmC^*_A; from the symmetry, the phase could also be SmC^*_{FI2} but this is highly unlikely at a lower temperature than SmC^*_{FI1}.

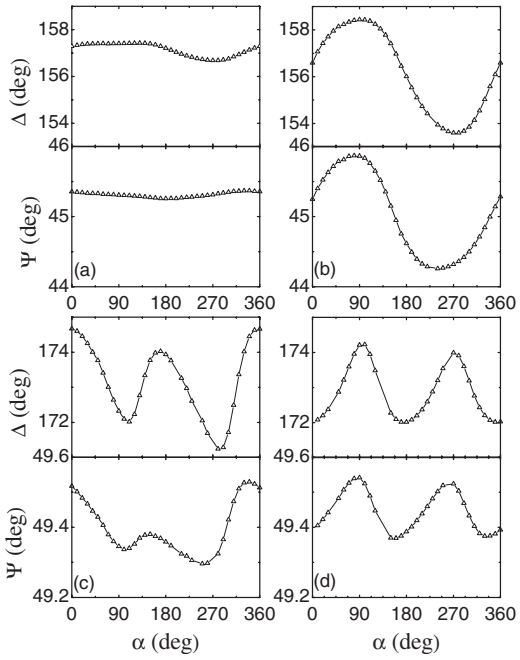

FIG. 5. Δ and Ψ vs α measured by NTE for each phase. Lines are guides for the eye. Data points are averages over 1 min at each orientation while the temperature was held constant at (a) 117.5 °C, (b) 112.9 °C, (c) 108.9 °C, and (d) 99.7 °C. The film thickness was 275 layers for (a) and (b) and 46 layers for (c) and (d).

V. RESONANT X-RAY DIFFRACTION

Resonant x-ray diffraction utilizes the presence of sulfur atoms in the molecules to gain information about molecular orientations [12,1]. The energy of synchrotron radiation (beamline X19A at NSLS) is tuned to the $K\alpha$ absorption edge of sulfur. The molecular structure factor then becomes a tensor sensitive to the orientations of the sulfur bonds [13], which are rigidly tied to the orientations of the molecular axes. When periodicity in the bond orientation exists, the tensor structure factor gives rise to resonant satellite peaks around the main Bragg peaks. The difference in the locations of the resonant peaks and the corresponding Bragg peaks in reciprocal space gives the periodicity of the molecular orientations. Again we use the freestanding film geometry with the sample in a temperature-controlled oven. A thick film is necessary to obtain strong diffraction peaks. The oven and the detector are mounted on the θ and 2θ rotation stages of a two-circle goniometer. When θ=0, the film plate and the smectic layers are in the plane of the synchrotron ring. The diffraction uses Bragg geometry, with the momentum transfer along the film normal, the $\hat{z}$ direction. The temperature was decreased from the SmA^* phase in steps. At each temperature, we scanned the (001) and (002) Bragg peaks and at least two resonant peaks to check for consistency.

Figure 6 shows scans at four different temperatures, representative of each phase [12]: 115.32 °C, 111.37 °C, 107.22 °C, and 103.10 °C. No resonant peaks were present at 115.65 °C and higher temperatures, in the SmA^* phase. In Fig. 6(a), the phase is SmC^*_α with an incommensurate helical pitch of 12.3 smectic layers. The resonant peaks are very close to the Bragg peak in Fig. 6(b), indicating that the phase is SmC^* with a pitch of 108 layers. The split resonant peak near Q_z/Q_o=4/3 in Fig. 6(c) shows an orientational periodicity of approximately three layers. The phase is SmC^*_{FI1}. The splitting of the resonant peak occurs because of distor-

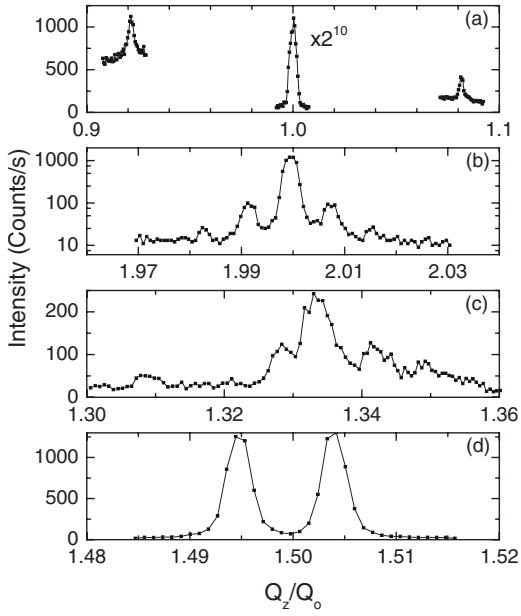

FIG. 6. Resonant peaks at (a) 115.32 °C, (b) 111.37 °C, (c) 107.22 °C, and (d) 103.10 °C. For each temperature, $Q_o=2\pi/d$, where d is the layer spacing, has been taken so that the (001) peak occurs at $Q_z/Q_o=1$. The (001) and (002) peaks are shown in (a) and (b) for comparison to the corresponding resonant peaks. Filter units were in place while scanning the (001) peak in (a), attenuating the intensity by a factor of 2^{10}.

tion from the clock model [14]. Both $m=\pm 1$ resonant peaks are shown in Fig. 6(d). The phase is SmC_A^* with the spacing between the resonant peaks due to a superimposed optical pitch of 137 layers. These results strongly support the phase sequence inferred by the rotational symmetry of the NTE data. The phase sequence is not consistent with the suggested phase sequence SmA^*-SmC_A^*-SmC^*-SmC_A^* in Ref. [5].

Beginning slightly above the SmA^*-SmC_α^* transition, the temperature was decreased in increments of 0.05 °C until the transition to the SmC^* phase. The pitch increases slowly with decreasing temperature from 12.3 layers at the SmA^*-SmC_α^* transition, as shown in Fig. 7. The magnitude of dP/dT increases as the SmC_α^*-SmC^* transition is approached. An abrupt jump in the pitch occurs at 114.96 °C. The differences in transition temperatures obtained by DOR, NTE, calorimetry, and RXRD are mainly due to calibrations of the thermometers. This is the first-order SmC_α^*-SmC^* transition observed by calorimetry. The layer spacing (Fig. 8) also has a discontinuity at the SmC_α^*-SmC^* transition. The temperature evolution of the pitch can also be extracted from the DOR data using the 4×4 matrix method [15]. In the 4×4 matrix method, each layer is modeled as a uniaxial slab with the optical axis along the average molecular axis. A transfer matrix formulation of Maxwell's equations is used to calculate the reflected and transmitted wave properties. The indices of refraction $n_o=1.516\pm0.004$ and $n_e=1.704\pm0.004$ for LN36 were extracted from NTE data for 56 films in the SmA^* phase [16]. The layer spacing was calculated by

$$d = d_A/\cos[A(T-T_{AC})^\beta],$$

where the untilted layer spacing $d_A=3.45$ nm was measured from the location of the Bragg peaks just above the

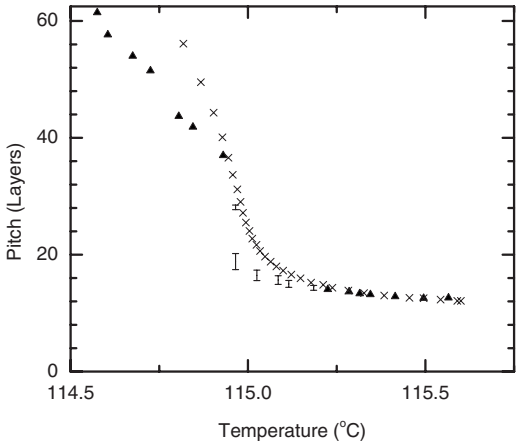

FIG. 7. Dependence of the helical pitch (solid triangles) on temperature around the SmC_α^*-SmC^* transition. In the coexistence region, the error bars represent the width of the resonant peaks. The crosses are the pitch values used to produce the simulation to the DOR data in Fig. 2.

SmA^*-SmC_α^* transition. The coefficient A and effective critical exponent $\beta=0.36$ were adjusted to fit I_P+I_S; the effective critical exponent is in agreement with extended mean field theory [17]. The number of surface layers and their tilt in the SmA^* phase were estimated by fitting NTE data with a synclinic surface layer structure. The amplitude of the I_P-I_S oscillations depends on the surface tilt, but not on the details of the surface structure. For the simulations shown in Fig. 2, we used a tilt that decreases exponentially with distance from the surface. The layers within the surface region were assumed to have synclinic tilts. The correlation length for both the tilt and azimuth surface organizations in the simulations increased linearly with temperature from 1.96 layers at 115.7 °C to 4.4 layers at 114.6 °C. Cusps or jumps in the DOR data occur whenever the net polarization of the film reaches zero [18,19], corresponding to a half integer number of turns of the helical pitch. The pitch was calculated at one

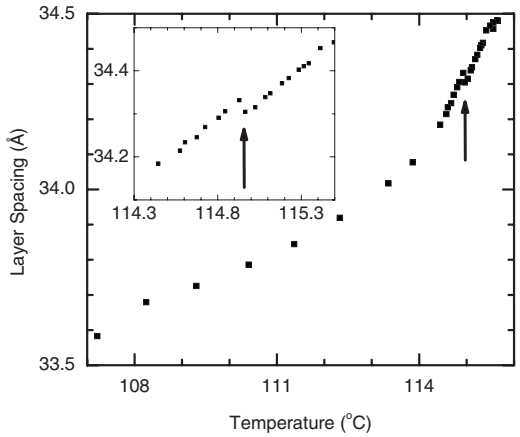

FIG. 8. Dependence of the smectic layer spacing with temperature. The layer spacing was calculated from the positions of the (001) and (002) peaks in reciprocal space. The inset shows the SmC_α^*-SmC^* transition in more detail. Arrows mark the discontinuity in the layer spacing at the SmC_α^*-SmC^* transition.

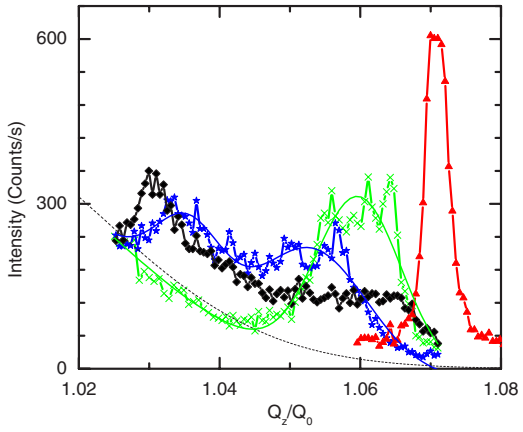

FIG. 9. (Color online) Resonant peaks at 115.29 °C (red triangles), 115.03 °C (green crosses), 114.97 °C (blue stars), and 114.93 °C (black diamonds). For all these data, $Q_o = 2\pi/3.4305$ nm^{-1}. The solid lines are Gaussian or double Gaussian fits of the number of counts above the background from the tail of the Bragg peak. The dotted line shows the background used for the Gaussian fits.

such point by comparing the pitch necessary to obtain a half integer number of turns with the x-ray pitch measurements. The pitch can then be calculated at all other temperatures using the fact that a complete oscillation in the DOR signal occurs when the number of turns changes by one. The pitch vs temperature obtained in this manner is shown along with the x-ray data in Fig. 7. They are in good agreement in the SmC^*_α phase until the point where the frequency of the DOR oscillations increases rapidly, indicating a large dP/dT. The discrepancy in the simulated and measured values of the pitch in the SmC^* phase is likely due to a rapid increase in the number of synclinic surface layers when the pitch becomes long.

Over the temperature region in which the DOR oscillations were rapid and of decreased amplitude, the x-ray scans also showed abnormal behavior. Scans of selected resonant peaks between 115.29 °C and 114.93 °C are shown in Fig. 9. At 115.29 °C, the scan was typical of the SmC^*_α phase with a pitch of 13.7 layers. The peak began to grow broad at 115.23 °C with lower maximum counts, though the integrated number of counts across the peak remained approximately the same. The width of the peak increased with decreasing temperature. At 114.97 °C, the peak resolved into two weak peaks superimposed on the background from the tail of the Bragg peak. The double Gaussian fit in Fig. 9 shows two distinct peaks. The two peaks represent two coexistent values of the pitch, 19 layers and 28 layers. Only one peak remains at 114.93 °C, in the SmC^* phase with a pitch of 37 layers.

Because the width of the resonant peak increases as temperature decreases between 115.23 °C and 115.03 °C before two separate peaks appear at 114.97 °C, we conclude that the primary reason for the increased width of the resonant peaks is the presence of two helices with differing pitch. The resonant peaks due to each helix are not quite resolved except at 114.97 °C. Another possible reason for the two peaks observed in the RXRD scan at 114.97 °C is that the longer pitch peak is due to the SmC^* phase, in which case the SmC^* and SmC^*_α phases would be shown to be coexistent. However, the peak at 115.03 °C shows no significant counts above the background at the location of the SmC^* peak, so we surmise that the higher pitch included in the peak at 114.97 °C evolves continuously from the peak at 115.03 °C. Both pitch values increase with decreasing temperature, with the higher pitch increasing more rapidly. The error bars in Fig. 7 show the width of the resonant peaks in this region. The two Gaussian fits at 114.97 °C are shown as two points in Fig. 7. We were not able to observe a phase boundary optically, as the helical pitch is shorter than the wavelength of visible light. The simulations from the DOR data agree fairly well with the higher pitch value over the entire region. The region over which the resonant peaks are abnormally broad coincides with the region over which the DOR oscillations had decreased amplitude. This raises the possibility that the decrease in amplitude is due to coexistent regions being probed simultaneously by the laser light.

The physical meaning of two different SmC^*_α pitch values is somewhat mysterious. One possibility is that surfaces contain a different pitch than the bulk. This is an unlikely explanation for our data because our RXRD setup typically requires films several hundred layers thick to obtain significant counts. Any surfaces are likely much too thin to be observed by RXRD. When surface effects are ruled out, two possibilities remain: domains with different helical pitch separated by defect lines or regions along the z axis in the bulk with different pitch. Both possibilities are consistent with our RXRD and DOR data. The presence of defect lines could be confirmed or eliminated by careful studies under cross polarizers. In addition, current theoretical models cannot explain coexistent SmC^*_α helices. The short pitch of the SmC^*_α phase is thought to be a result of frustration between interactions with nearest neighbor layers and next nearest neighbor layers [20], resulting in a minimum in the free energy at a single value of the pitch. Coexistent pitches indicate that two local minima in the free energy are present.

VI. CONCLUSIONS

Our measurements rule out the antiferroelectric-ferroelectric-antiferroelectric phase transition suggested in Ref. [5]. DOR, NAS calorimetry, NTE, and RXRD all concur that the phase sequence for LN36 is SmA^*-SmC^*_α-SmC^*-SmC^*_{FI1}-SmC^*_A. The phase showing antiferroelectriclike behavior in Ref. [5] above the SmC^* is SmC^*_α. The short helical pitch of the SmC^*_α can give antiferroelectriclike response, but the phase could be more accurately described as helielectric.

RXRD and NAS calorimetry clearly show that the SmC^*_α-SmC^* transition is first order with a relatively small discontinuity in the pitch. In addition, unusual pretransitional effects occur in the SmC^*_α phase. Two coexistent values of the helical pitch were present. The unusual oscillations in the DOR signal may be a result of the coexistent helices.

ACKNOWLEDGMENTS

We are grateful to P. Barois for lending us his x-ray oven for the RXRD studies. Research at NSLS, BNL was supported in part by the U. S. Department of Energy, Division of Materials Sciences and Division of Chemical Sciences, under Contract No. DE-AC02-98CH10886. The research was supported in part by the donors of the Petroleum Research Fund, administered by the American Chemistry Society and by the National Science Foundation, Solid State Chemistry Program under Grants No. DMR-0106122 and No. DMR-0605760. B.K.M. and Z.Q.L. acknowledge support from the University of Minnesota Graduate School.

[1] L. S. Hirst, S. J. Watson, H. F. Gleeson, P. Cluzeau, P. Barois, R. Pindak, J. Pitney, A. Cady, P. M. Johnson, C. C. Huang, A-M. Levelut, G. Srajer, J. Pollmann, W. Caliebe, A. Seed, M. R. Herbert, J. W. Goodby, and M. Hird, Phys. Rev. E **65**, 041705 (2002).

[2] V. Laux, N. Isaert, V. Faye, and H. T. Nguyen, Liq. Cryst. **27**, 81 (2000).

[3] E. Gorecka, D. Pociecha, M. Čepič, B. Žekš, and R. Dabrowski, Phys. Rev. E **65**, 061703 (2002).

[4] Z. Q. Liu, S. T. Wang, B. K. McCoy, A. Cady, R. Pindak, W. Caliebe, K. Takekoshi, K. Ema, H. T. Nguyen, and C. C. Huang, Phys. Rev. E **74**, 030702(R) (2006).

[5] S. K. Kundu, B. K. Chaudhuri, A. Seed, and A. Jákli, Phys. Rev. E **67**, 041704 (2003).

[6] S. Pankratz, P. M. Johnson, and C. C. Huang, Rev. Sci. Instrum. **71**, 3184 (2000).

[7] H. Yao, K. Ema, and C. W. Garland, Rev. Sci. Instrum. **69**, 172 (1998).

[8] K. Ema and H. Yao, Thermochim. Acta **304/305**, 157 (1997).

[9] P. M. Johnson, D. A. Olson, S. Pankratz, Ch. Bahr, J. W. Goodby, and C. C. Huang, Phys. Rev. E **62**, 8106 (2000).

[10] D. A. Olson, X. F. Han, P. M. Johnson, A. Cady, and C. C. Huang, Liq. Cryst. **29**, 1521 (2002).

[11] P. M. Johnson, D. A. Olson, S. Pankratz, T. Nguyen, J. Goodby, M. Hird, and C. C. Huang, Phys. Rev. Lett. **84**, 4870 (2000).

[12] P. Mach, R. Pindak, A.-M. Levelut, P. Barois, H. T. Nguyen, C. C. Huang, and L. Furenlid, Phys. Rev. Lett. **81**, 1015 (1998).

[13] A.-M. Levelut and B. Pansu, Phys. Rev. E **60**, 6803 (1999).

[14] A. Cady, J. A. Pitney, R. Pindak, L. S. Matkin, S. J. Watson, H. F. Gleeson, P. Cluzeau, P. Barois, A.-M. Levelut, W. Caliebe, J. W. Goodby, M. Hird, and C. C. Huang, Phys. Rev. E **64**, 050702(R) (2001).

[15] D. W. Berreman, J. Opt. Soc. Am. **62**, 502 (1972); H. Wohler, G. Haas, M. Fritsch, and D. A. Mlynski, J. Opt. Soc. Am. A **5**, 1554 (1988).

[16] C. C. Huang, S. T. Wang, X. F. Han, A. Cady, R. Pindak, W. Caliebe, K. Ema, K. Takekoshi, and H. Yao, Phys. Rev. E **69**, 041702 (2004).

[17] C. C. Huang and J. M. Viner, Phys. Rev. A **25**, 3385 (1982).

[18] D. Schlauf, Ch. Bahr, and H. T. Nguyen, Phys. Rev. E **60**, 6816 (1999).

[19] P. M. Johnson, S. Pankratz, P. Mach, H. T. Nguyen, and C. C. Huang, Phys. Rev. Lett. **83**, 4073 (1999).

[20] A. Cady, D. A. Olson, X. F. Han, H. T. Nguyen, and C. C. Huang, Phys. Rev. E **65**, 030701(R) (2002); V. P. Panov, B. K. McCoy, Z. Q. Liu, J. K. Vij, J. W. Goodby, and C. C. Huang, *ibid.* **74**, 011701 (2006).